ELSEVIER

Journal of Power Sources 81–82 (1999) 685–689

JOURNAL OF POWER SOURCES

www.elsevier.com/locate/jpowsour

Direct XRD observation of oxidation-state changes on Li-ion insertion into transition-metal oxide hosts

Ö. Bergström, H. Björk, T. Gustafsson, J.O. Thomas *

Inorganic Chemistry, Ångström Laboratory, Uppsala University, Box 538, SE-751 21 Uppsala, Sweden

Abstract

It is demonstrated here that the electron redistribution occurring as lithium becomes incorporated into or extracted from a crystalline transition-metal oxide (TMO) host can be studied experimentally by single-crystal X-ray diffraction (XRD) for the case of V_6O_{13}. The crystals pass through a sequence of $Li_xV_6O_{13}$ phases ($x = 0$, 0.5, 1, 2, 3 and 6) as lithium ions are incorporated into the V_6O_{13} structure on discharging a $\langle$Li|liquid electrolyte|$V_6O_{13}\rangle$ cell from 3.2 to 1.8 V. The so-called deformation electron-density refinement of the electron distribution is exploited to extract the number of electrons associated with the Li, V and O atoms in the structure, and hence the electron rearrangement taking place on lithium insertion. This type of study is ultimately capable of identifying the complete sequence of oxidation-state changes occurring during the entire lithium insertion process in V_6O_{13}.

Keywords: Vanadium oxide; Cathode material; Lithium insertion mechanism; In situ X-ray diffraction; Deformation electron density refinement

1. Introduction

The transition-metal oxide V_6O_{13} is a particularly interesting cathode material for high-capacity lithium-polymer battery applications in conjunction with a metallic lithium anode. The electrochemical properties of V_6O_{13} have their origin in the open nature of its crystal structure, thus facilitating lithium-ion diffusion, combined with the fact that vanadium ions can readily change their oxidation state on lithium-ion insertion. V_6O_{13} was first suggested as a useful cathode material by Murphy et al. [1]. Its crystal structure was studied as early as 1948 [2], and further refined by Wilhelmi et al. [3]. It comprises alternating layers of two types parallel to the ab-plane: a single layer of edge-sharing VO_6 octahedra at $z = 0$ (incorporating vanadium V1 of the asymmetric unit), and a similar double layer at $z = 0.5$ involving V2 and V3. The two layers are connected via corner-sharing oxygens O5 and O6 (Fig. 1).

In a battery context, lithium ions insert into the V_6O_{13} particles of the composite cathode of a $\langle$Li|liquid or polymer electrolyte|$V_6O_{13}\rangle$ cell during discharge. V_6O_{13} thus passes through a sequence of discrete lithiated phases, $Li_xV_6O_{13}$. The stepwise nature of the discharge curve, with the quasi-vertical sections corresponding to single-phase compositions, and the plateau-like sections to two-phase regions, is shown in Fig. 2. Several earlier investigations have been made of the lithiated phases; see Table 1. Some were based on chemically lithiated materials, while others were ex situ studies of dismantled cells. In this present work, single-crystal and in situ powder X-ray diffraction techniques have been combined for electrochemically lithiated samples to achieve a more complete understanding of the electrochemical behaviour of V_6O_{13} as a lithium insertion material.

The limited resolution of our earlier described in situ X-ray powder diffraction technique [6] has not facilitated the determination of the structural rearrangement brought about by lithium-ion insertion. The situation is now improved by several orders of magnitude through the use of single-crystal XRD techniques. The data so derived has proved to be of sufficient accuracy as to provide information relating to oxidation-state changes affecting individual vanadium and oxygen atoms. Here, the method is illustrated only for the case of V_6O_{13} and $Li_2V_6O_{13}$.

* Corresponding author. E-mail: josh.thomas@kemi.uu.se

0378-7753/99/$ - see front matter
PII: S0378-7753(98)00231-6

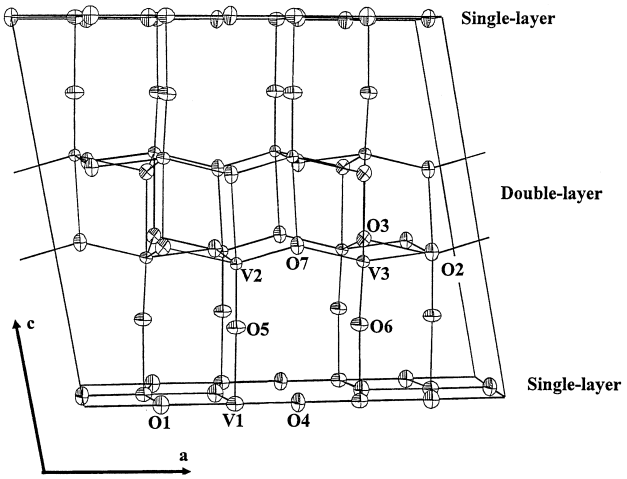

Fig. 1. The crystal structure of V_6O_{13} viewed along the *b*-axis. Thermal ellipsoids are drawn at a 90% level of probability.

2. Experimental

2.1. Growth of V_6O_{13} single crystals

V_6O_{13} powder samples were prepared by controlled thermal decomposition of ammonium vanadate (NH_4VO_3) powder [8,9]. This powder was incorporated into the composite cathode of flat 'coffee-bag'-type cells, and also used as seed-material for the synthesis of larger single crystals for the XRD electron density studies. This synthesis was performed by chemical vapour transport (CVT). The starting material was a 20:1 mass-ratio mixture of crystallographically phase-pure V_6O_{13} powder and $TeCl_4$ (Merck: as received) [10].

Table 1
Earlier suggestions for the phases formed during the lithiation of V_6O_{13}

x in $Li_xV_6O_{13}$	Reference
0.95, 2.75, 3.65, 6.05	Abraham et al. [4]
1, 3, 4, 8	West et al. [5]
1, 4, 8	Gustafsson et al. [6]
0.5, 1.5, 3, 6	Lampe-Önnerud et al. [7]

2.2. Lithiation of V_6O_{13} single crystals

Electrochemical lithiation of V_6O_{13} single crystals was achieved by incorporating an identifiable set of ca. 0.1 mm max. dim. single crystals into the composite cathode of a $\langle$Li|liquid electrolyte|$V_6O_{13}\rangle$ fraction. This was carried out under a microscope in a dry-argon glovebox (<1 ppm O_2/H_2O). The cell was maintained at a slightly elevated temperature (ca. 50°C) in a thermostatically controlled sand-bath (to enhance reaction kinetics and lithium-ion diffusion) during discharge from an initial 3.0 V vs. Li/Li^+ over a period of ca. 6 weeks using a MacPile™ potentiostat (Fig. 3). The lithiated single crystals were then recovered from the cathode and mounted on an X-ray goniometer, again under a microscope in a dry-argon filled glovebox.

2.3. Single-crystal X-ray diffraction

Single-crystal X-ray diffraction data were collected both on V_6O_{13} and on a crystal electrochemically lithiated at 2.65 V vs. Li/Li^+ using a Stoe & Cie 4-circle single-crystal X-ray diffractometer (Mo $K\alpha_1$ radiation); the data-sets were collected at room temperature (22°C), and the peaks scanned in a $\theta/2\theta$-mode ($\Delta\theta = 0.01°$ for 70 steps). Standard reflections were measured every 240 min

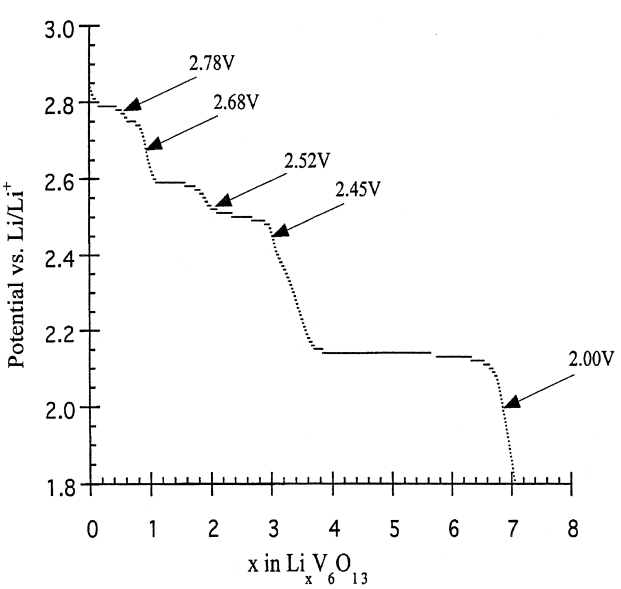

Fig. 2. Discharge curve of a $\langle$Li|polymer electrolyte|$V_6O_{13}\rangle$ cell.

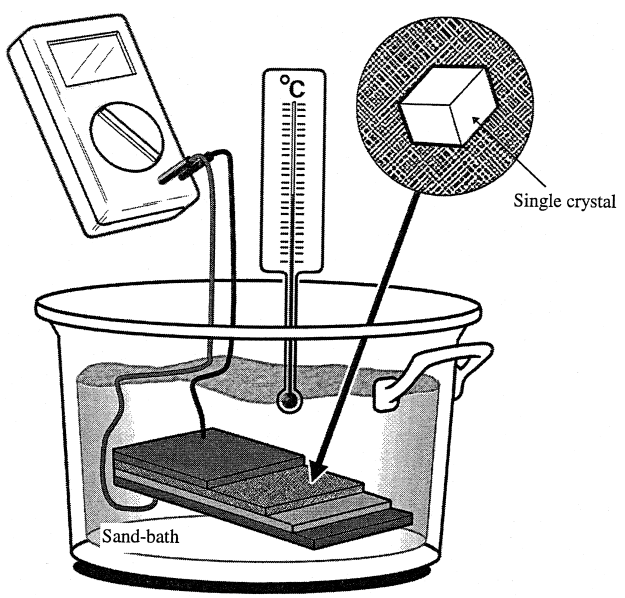

Fig. 3. Experimental set-up for the electrochemical lithiation of single crystals.

Table 2
Single-crystal data collection and refinement details

	V_6O_{13}	$Li_2V_6O_{13}$
Transmission (max.)	0.591	0.679
Transmission (min.)	0.448	0.323
2θ-max. (°)	100	105
No. of independent reflections	2455	2876
No. of measured reflections	4972	5730
Internal $R(F^2)$ (%)	2.8	3.0
No. of parameters refined (conventional model)	65	71
No. of parameters refined (deformation model)	68	75
$wR(F^2)$ (conv. ref.) (%)	5.3	5.5
$wR(F^2)$ (def. ref.) (%)	4.4	4.2

during the data collections. The intensities and their standard deviations were corrected for background, time-dependent variations, and for polarisation and absorption effects; see Table 2 for details of the data collections.

2.4. Deformation electron density refinement

In conventional refinement of single-crystal X-ray diffraction data, the calculated structure factors are generally based on the use of spherical neutral-atom X-ray atomic scattering form factors. This procedure is quite adequate for crystal structure refinement. However, such a model ignores the existence of different oxidation states and non-spherical electron distributions (lone-pairs, bonding-electron densities, etc.) in the structure. Such effects can be included in so-called deformation electron density refinement, in which the deviation of the electron density, $\delta\rho(r)$, for each atom from a spherical neutral-atom distribution is modelled by a linear combination of deformation functions. The method was first proposed by Hirshfeld [11], in which:

$$\delta\rho(r) = \sum_{n=0}^{4} \sum_{k=1}^{(n+1)(n+2)/2} c_{n,k}\,\rho_{n,k}(r)$$

where $\rho_{n,k}(r) = N_n r^n \exp(-\gamma r^2)\cos^n\theta_k$. This implies the possible use of up to 35 functions in the most general case, were N_n is a normalisation factor, and r and θ_k are polar coordinates. The deformation models used here included only spherical, linear and quadratic terms ($n = 0$, 1 and 2) for the $x = 0$ and 2 cases. Mirror-symmetry constraints (mirror in $y = 0$ plane) were applied to these functions for

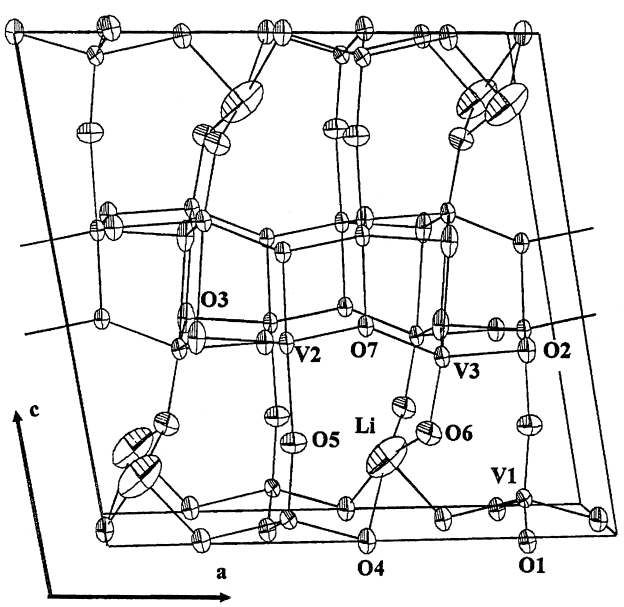

Fig. 4. The structure of $Li_2V_6O_{13}$. Thermal ellipsoids are drawn at a 90% level of probability.

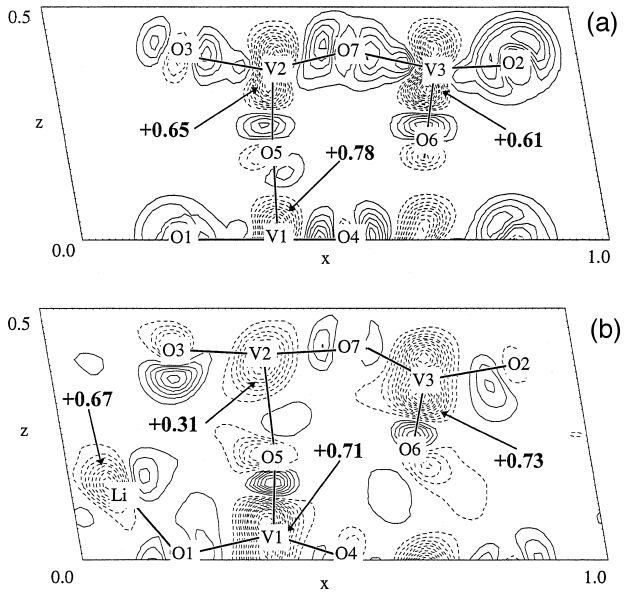

Fig. 5. Deformation electron density map at $y = 0$ in the ac-plane for (a) V_6O_{13} and (b) $Li_2V_6O_{13}$. Contour intervals at 0.05 e/Å^3; negatively charged regions are drawn as solid lines; positive regions are dashed; the zero-level is omitted.

Table 3
Ionic charges associated with refined charge deformation model

Atom	V_6O_{13}/e	$Li_2V_6O_{13}$/e	'$Li_2V_6O_{13}$ − V_6O_{13}'/e
Li	–	0.67(15)	+0.67
V1	0.78(17)	0.71(14)	−0.07
V2	0.65(15)	0.31(14)	−0.34
V3	0.61(15)	0.73(14)	+0.12
O1	−0.48(13)	−0.67(10)	−0.19
O2	−0.65(8)	−0.68(10)	−0.03
O3	−0.35(9)	−0.60(10)	−0.25
O4	−0.30(14)	0.13(15)	+0.43
O5	−0.06(10)	−0.18(11)	−0.12
O6	−0.10(11)	−0.31(11)	−0.21
O7	−0.33(10)	−0.11(10)	+0.22

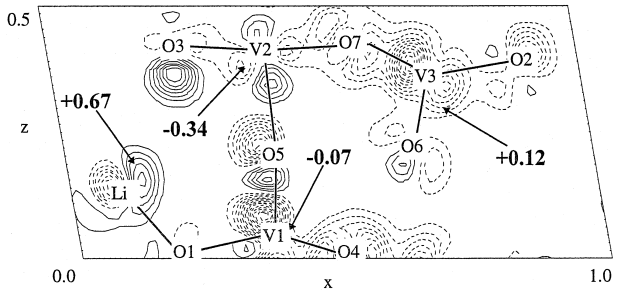

Fig. 6. '$Li_2V_6O_{13}$–V_6O_{13}' difference deformation electron density map in the ac-plane at $y = 0$; contours plotted as in Fig. 5.

all atoms in the structures, giving a total of only seven $c_{n,k}$ parameters to be refined for each atom. Local coordinate systems for the deformation functions are defined individually for each atom, and in the same way for V_6O_{13} and $Li_2V_6O_{13}$. The overall γ-value (describing the radial charge distribution for each atom) was optimised empirically to 4.0. The precise value of γ does not influence the refinements significantly. After convergence, the effective charge associated with each atom is given directly as the sum of the refined $c_{n,k}$-values for n-even deformation functions; n-odd $c_{n,k}$-values contribute zero charge. All refinements were performed using the DUPALS program package described by Lundgren [12]. The electron redistribution resulting from lithium insertion into V_6O_{13} is given by the 'difference' deformation electron density, whereby the refined coefficients, $c_{n,k}$, for V_6O_{13} are subtracted term-by-term from the $c_{n,k}$-values obtained for the refinement of the $Li_2V_6O_{13}$ structure.

3. Results and discussion

The structures of the $x = 0$ and $x = 2$ cases are closely similar and can be described in terms of two types of layer in the ab-plane. The first involves a single layer of edge-sharing VO_6 octahedra at $z = 0$ incorporating V1; the second is a double layer at $z = 0.5$ involving V2 and V3. The two layers are connected via corner-sharing oxygens O5 and O6 (Fig. 1).

3.1. The $Li_2V_6O_{13}$ structure

Lithium is inserted between the single- and double-layers of the V_6O_{13} structure, and coordinate to oxygens within the single-layer and to the oxygens between the layers (Fig. 4). This results in a 7.6% c-axis expansion with respect to V_6O_{13}. The lithium ion has a five-fold oxygen coordination in a tetragonal pyramid with Li–O distances in the range 1.95–2.46 Å. For a more complete description, including atomic coordinates and distances, see Ref. [13].

3.2. The difference deformation electron density for '$Li_2V_6O_{13}$–V_6O_{13}'

The difference deformation electron densities for all three vanadium atoms (V1, V2 and V3) in V_6O_{13} (Fig. 5a) have a generally similar appearance, with dumb-bell shaped regions of electron deficiency extending roughly in the c-direction. The effective ionic charges on the vanadium atoms are: +0.78(17), +0.65(15) and +0.61(15) for V1, V2 and V3, respectively (Table 3). The oxygen atoms within the single- and double-layers are each associated with two regions of electron excess in the $+a$ and $-a$ directions. Oxygens O5 and O6, located between the layers, are also associated with regions of electron excess in the $+c$ and $-c$ direction, with O6 exhibiting some degree of dipolar character.

In $Li_2V_6O_{13}$, the deformation electron density associated with vanadium atoms V1 and V3 have a similar dumb-bell shaped appearance, with the regions of electron deficiency extending roughly in the c-direction (Fig. 5b). However, vanadium V2 is associated with a spherical region of electron deficiency. The effective ionic charges on the vanadium atoms are: +0.71(14), +0.31(14) and +0.73(14) for V1, V2 and V3, respectively (Table 3). Oxygen O3 is associated with a large positive lobe extending in the direction of the inserted lithium ions, and a negative lobe extending in the opposite direction.

The difference deformation electron density map ('$Li_2V_6O_{13}$–V_6O_{13}') (Fig. 6) shows the vanadium atoms

Table 4
Proposed sequence of vanadium oxidation states in $Li_xV_6O_{13}$

	V_6O_{13}	$Li_{0.5}V_6O_{13}$	$Li_1V_6O_{13}$	$Li_2V_6O_{13}$	$Li_3V_6O_{13}$	$Li_6V_6O_{13}$	$(Li_8V_6O_{13})^*$
V1	$4^+4^+4^+4^+$	$4^+4^+4^+4^+$	$4^+4^+4^+4^+$	$4^+4^+4^+4^+$	$3^+3^+4^+4^+$	$3^+3^+3^+3^+$	$3^+3^+3^+3^+$
V2	$5^+5^+5^+5^+$	$4^+5^+5^+5^+$	$4^+4^+5^+5^+$	$4^+4^+4^+4^+$	$4^+4^+4^+4^+$	$4^+4^+4^+4^+$	$3^+3^+3^+3^+$
V3	$4^+4^+4^+4^+$	$4^+4^+4^+4^+$	$4^+4^+4^+4^+$	$4^+4^+4^+4^+$	$4^+4^+4^+4^+$	$3^+3^+3^+3^+$	$3^+3^+3^+3^+$

* Not observed in this work.

V1 and V3 to be surrounded by regions of electron deficiency, while vanadium V2 is surrounded by both positive and negative regions. The change in charge for the V2 atom from $+0.65(15)$ to $+0.31(14)$ as lithium is inserted is seen to be the only significantly observed effect. The corresponding values for V1 and V3 are from $+0.78(17)$ to $+0.71(14)$ for V1, and from $+0.61(15)$ to $+0.73(14)$ for V3. This suggests that V2 undergoes a change in formal oxidation-state (nominally, from $+5$ to $+4$ if such a simplistic mode indeed has any practical relevance), while V1 and V3 remain unchanged at $+4$. It is a common experience in deformation electron density studies that full formal charges ($+5$ and $+4$ in this case) are never found experimentally; the charge is shared with the nearest-neighbour oxygen surroundings. It can be noted in this connection that recent ab initio calculations of electron densities for related materials have shown that much of the charge transferred on lithium insertion is indeed accumulated on the oxygen atoms in the structures [14]. In fact, it is found that O3 is here associated with a large region of electron deficiency in the direction of the lithium ion, and with an effective change in charge from $-0.35(9)$ to $-0.60(10)$ in going from V_6O_{13} to $Li_2V_6O_{13}$.

4. Conclusion

The exploitation of this method to study the entire sequence of $Li_xV_6O_{13}$ phases is now underway. While a more complete discussion lies outside the scope of this present paper, a tentative proposal is emerging for the entire sequence of oxidation-state changes for vanadium ions during the lithium insertion process. This is included here (for the interest of the reader) in Table 4.

Acknowledgements

This work has been supported by *The Swedish Natural Science Research Council* (NFR) and *The Swedish Board for Technical Development* (NUTEK). The authors also wish to thank Steen Yde-Andersen and René Koksbang of Danionics A/S, Odense, Denmark for their support and interest in this work.

References

[1] D.W. Murphy, P.A. Christian, F.J. DiSalvo, J.N. Carides, J. Electrochem. Soc. 126 (1979) 497.
[2] F. Aebi, Helv. Chim. Acta 31 (1948) 8.
[3] K.A. Wilhelmi, K. Waltersson, L. Kihlborg, Acta Chem. Scand. 25 (1971) 2675.
[4] K.M. Abraham, J.L. Goldman, M.D. Dempsey, J. Electrochem. Soc. 128 (1981) 2493.
[5] K. West, B. Zachau-Christiansen, T. Jacobsen, S. Atlung, J. Power Sources 14 (1985) 235.
[6] T. Gustafsson, J.O. Thomas, R. Koksbang, G.C. Farrington, Electrochim. Acta 37 (1992) 1639.
[7] C. Lampe-Önnerud, J.O. Thomas, M. Hardgrave, S. Yde-Andersen, J. Electrochem. Soc. 142 (1995) 3648.
[8] C. Lampe-Önnerud, J.O. Thomas, Eur. J. Sol. State and Inorg. Chem. 32 (1995) 293.
[9] N.C. Chaklanabish, H.S. Maiti, J. Thermal Anal. 31 (1986) 1243.
[10] M. Saeki, N. Kimizuka, I. Ishii, I. Kawada, M. Nakano, A. Ichinose, M. Nakahira, J. Cryst. Growth 18 (1973) 101.
[11] F.L. Hirshfeld, Acta Cryst. B 27 (1971) 769.
[12] J.-O. Lundgren, Crystallographic Computing Programs, Report UUIC-B13-405, Institute of Chemistry, Univ. of Uppsala, Sweden, 1983.
[13] Ö. Bergström, T. Gustafsson, J.O. Thomas, Acta Crystallogr. C 53 (1997) 528.
[14] M.K. Aydinol, A.F. Kohan, G. Ceder, K. Cho, J. Joannopoulos, Phys. Rev. B 56 (1997) 1354.